Hindawi International Journal of Aerospace Engineering Volume 2022, Article ID 5352146, 18 pages https://doi.org/10.1155/2022/5352146



Review Article

Review of Root-Mean-Square Error Calculation Methods for Large Deployable Mesh Reflectors

Sichen Yuan (1)

A. Leon Linton Department of Mechanical, Robotics and Industrial Engineering, Lawrence Technological University, MI 48075-1058, USA

Correspondence should be addressed to Sichen Yuan; syuan@ltu.edu

Received 26 March 2022; Revised 24 May 2022; Accepted 8 July 2022; Published 4 August 2022

Academic Editor: Adel Ghenaiet

Copyright © 2022 Sichen Yuan. This is an open access article distributed under the Creative Commons Attribution License, which permits unrestricted use, distribution, and reproduction in any medium, provided the original work is properly cited.

In the design of a large deployable mesh reflector, high surface accuracy is one of ultimate goals since it directly determines overall performance of the reflector. Therefore, evaluation of surface accuracy is needed in many cases of design and analysis of large deployable mesh reflectors. The surface accuracy is usually specified as root-mean-square error, which measures deviation of a mesh geometry from a desired working surface. In this paper, methods of root-mean-square error calculation for large deployable mesh reflectors are reviewed. Concept of reflector gain, which describes reflector performance, and its relationship with the root-mean-square error is presented. Approaches to prediction or estimation of root-mean-square error in preliminary design of a large deployable mesh reflector are shown. Three methods of root-mean-square error calculation for large deployable mesh reflectors, namely, the nodal deviation root-mean-square error, the best-fit surface root-mean-square error, and the direct root-mean-square error, are presented. Concept of effective region is introduced. An adjusted calculation of root-mean-square error is suggested when the concept of effective region is involved. Finally, these reviewed methods of root-mean-square error calculation are applied to surface accuracy evaluation of a two-facet mesh geometry, a center-feed mesh reflector, and an offset-feed mesh reflector for demonstration and comparison.

1. Introduction

Large deployable mesh reflectors (DMRs), due to their important space applications, have experienced continued research and development interest in the past several decades [1–4]. A deployable mesh reflector uses a spherical or parabolic surface as a working shape (a required radiofrequency surface), which is formed by a network or mesh of tensioned facets.

A DMR in consideration is illustrated in Figure 1, which, after full deployment, is supported by a stiff and stable flat frame. Although there are some variations, a typical DMR is composed of a front cable net, a rear cable net, tension ties, and a supporting structure. The front net (working surface) in the figure, as well as the rear net, is constructed by a mesh of flat triangular facets. Edges of the facets are elastic cable elements interconnected at facet nodes. The nodes of the front and rear nets are also connected by tension ties of adjustable lengths. In setting up the DMR, folded nets are

deployed into highly stretched elastic meshes, with lengths of the tension ties being properly adjusted such that the facets of the front net eventually form a working surface that is approximate to the desired radiofrequency surface.

In the design of a large DMR, high surface accuracy is one of the ultimate goals since it directly determines overall performance of the reflector. Therefore, evaluation of surface accuracy is needed in many cases of design and analysis of large DMRs. For example, surface accuracy can be either roughly estimated in preliminary design of a DMR to determine topology, member materials, and facet sizes [1, 5] or accurately evaluated for analysis of generated mesh geometry [1, 6]. The surface accuracy is usually specified as rootmean-square (RMS) error, which measures deviation of the mesh geometry from the desired working surface.

In this paper, commonly used state-of-the-art methods of RMS error calculation for large DMRs shall be reviewed. Methods to be reviewed include approaches to both rough

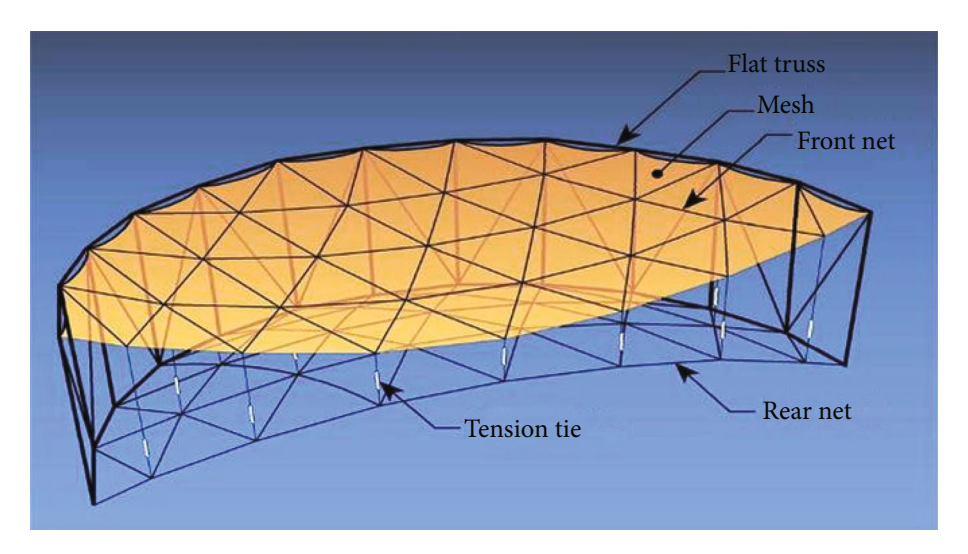


FIGURE 1: A typical DMR with deployed working surface.

estimation of RMS error for preliminary design and accurate calculation of RMS error for performance evaluation of large DMRs. Concepts of reflector gain and effective region, and their relationship with RMS error calculation shall also be reviewed. A comprehensive mathematical description shall be given for each method introduced. The reviewed methods shall be implemented both in a simple example for illustrative purpose and in practical examples for validation of engineering applicability.

The remainder of this paper is organized as follows: concept of reflector gain, which is a factor that describes reflector performance, and its relationship with RMS error calculation will be presented in Section 2. Methods of RMS error prediction in preliminary DMR design will be introduced in Section 3. Method of RMS error calculation for generated mesh geometries of DMRs will be described in Section 4. Concept of effective region and the corresponding incorporation in RMS error calculation will be shown in Section 5. Reviewed methods of RMS error calculation will be applied to evaluate surface accuracies of several mesh geometries for demonstration and comparison in Section 6. Conclusions of the reviewed methods of RMS error calculation will be given in Section 7.

2. Reflector Gain and RMS Effective Surface Error

Gain of a reflector is a factor that describes reflector performance. It is essential to obtain a reflector with high gain since loss of gain will seriously reduce efficiency in signal transmission. An axial gain of a circular aperture may be written as [7]

$$G = G_0 e^{-\bar{\delta}^2}, \quad \bar{\delta} = \frac{4\pi\varepsilon}{\lambda}.$$
 (1)

where G_0 is the gain of no-error reflecting surface with the value being $\eta_{\rm eff} (\pi D/\lambda)^2$. $\eta_{\rm eff}$ is the aperture efficiency. D is

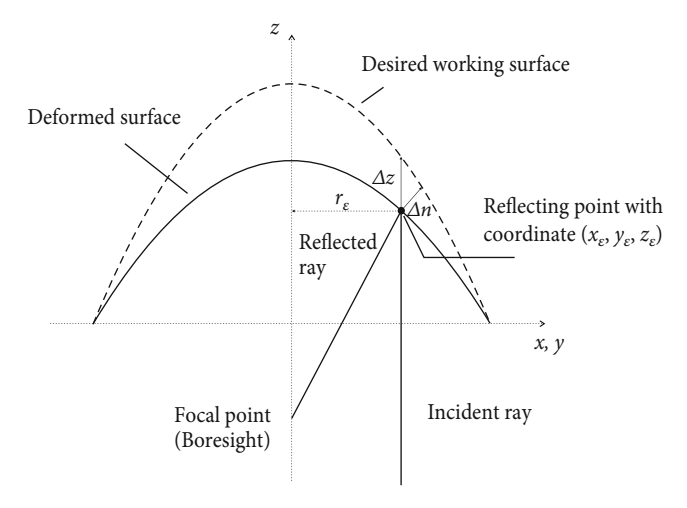


FIGURE 2: Geometric information of surface deviations in the z-direction and in the direction normal to the reflecting surface.

the aperture diameter. λ is the wavelength. $\bar{\delta}$ is the illumination weighted mean phase error. ε is called half-path-length error [8] or effective surface error [7] of a reflecting point on the reflecting surface with coordinate $(x_{\varepsilon}, y_{\varepsilon}, z_{\varepsilon})$ (see Figure 2). In Equation (1), it is assumed that random reflector surface deformation is much smaller than the wavelength.

A relationship between reflector gain and half-path-length error is described in Equation (1), which indicates that large surface error significantly deteriorates gain of a reflector, which was first found out by Spencer [9]. According to Ruze [7], ε may be obtained by Equations (2a) and (2b) with a measurement of a surface deviation Δz in the z-direction or a surface deviation Δn in the direction normal to the reflecting surface (see Figure 2).

$$\varepsilon = \frac{\Delta z}{1 + (r_{\varepsilon}/2F)^2},\tag{2a}$$

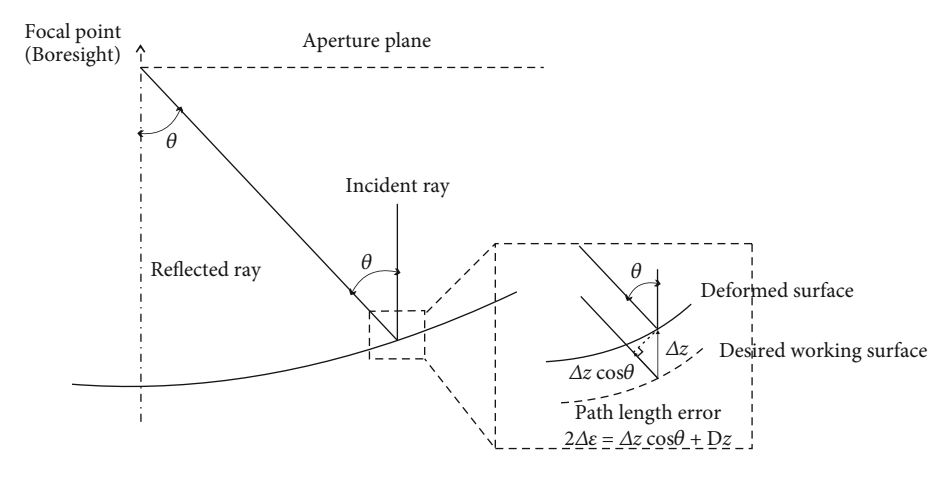


FIGURE 3: Geometric relation between path length error and antenna surface deformation from Ref. [8].

$$\varepsilon = \frac{\Delta n}{\sqrt{1 + (r_{\varepsilon}/2F)^2}},\tag{2b}$$

where F is the focal length of a reflector and $r_{\varepsilon} = \sqrt{x_{\varepsilon}^2 + y_{\varepsilon}^2}$ is the distance from this given reflecting point to the center of a reflector in the xy-plane.

According to Tanaka [8], ε may also be obtained by Equation (3)

$$\varepsilon = \frac{(1 + \cos \theta) \Delta z}{2}.$$
 (3)

Figure 3 shows the geometric information of ε . In this figure, θ is the angle between focal point direction and direction from a reflecting point on the reflector to the focal point.

Note that in Equations (2a), (2b), and (3), ε is defined as surface error of a specific reflecting point within a reflector aperture. To evaluate surface error of the whole reflector, a root-mean-square effective surface error is defined in [10, 11]

$$\varepsilon_{\rm rms} = \sqrt{\frac{\iint_{S'} \varepsilon(x, y)^2 \psi dS'}{\iint_{S'} \psi dS'}},\tag{4}$$

where ψ is an "illumination function" which sometimes is assumed uniform with $\psi = 1$ [11]. S' is aperture area of the reflector.

3. RMS Error Prediction in Preliminary Design of DMRs

For a large DMR whose reflecting surface is formed by facets, it is essential to predict surface accuracy of the DMR before a mesh geometry is fully generated. Facet sizes need to be known in preliminary design, such that numbers of nodes and facets can be determined. Different from the root-mean-square half-path-length error $\varepsilon_{\rm rms}$, which measures deviation of a deformed reflecting surface from a

desired working surface of general reflectors, the root-mean-square flat facets error $\delta_{\rm rms}$ is used to evaluate deviation of a mesh geometry from a desired working surface. $\delta_{\rm rms}$ is defined to have the same unit of wavelength λ . Depending on applications, different budgets for surface accuracy related to the facet geometry are suggested as follows [6, 12]:

$$\delta_{\rm rms} \le \frac{\lambda}{N},$$
 (5)

where N = 50, 75, 100, 150, or 200. Surface deviation of a DMR may be caused by geometric difference between flat facets and desired working surface (say, a parabolic or spherical surface), variation of tension tie load, member length imperfection, ring structure distortion, and/or thermal strain.

A link between δ_{rms} and gain/loss estimation can be obtained by an approach similar to Equation (1) [13]:

$$\eta_{\rm rms} = \exp\left[-\left(\frac{4\pi\delta_{\rm rms}}{\lambda}\right)^2\right],$$
(6)

where $\eta_{\rm rms}$ is the efficiency factor of reflector gain due to the RMS error. The reflector gain estimation due to the RMS error can be obtained as

$$G = \eta_{\rm rms} G_0. \tag{7}$$

Although Ruze's derivation in Equation (1) assumes random surface errors, it was proved that the approach in Equation (6) is also useful for estimating gain/loss from systematic error sources [14].

Agrawal et al. [1] proposed a technique to predict RMS error for a mesh reflector. RMS error $\delta_{rms-pre}$ in preliminary design is estimated in Equation (8) as

$$\delta_{\text{rms-pre}} = \frac{1}{8\sqrt{15}} \frac{L^2}{R}.$$
 (8)

Note that this approximation is obtained under two assumptions: first, the desired working surface is a sphere with radius being R; second, all facets are equilateral triangles with the lengths of three sides being L. Then, the allowable length of facet edge is calculated as

$$\frac{L}{D} = 4\sqrt[4]{15}\sqrt{\frac{\delta_{\text{rms-pre}}F}{D}}.$$
 (9)

Reference [1] also introduced an RMS error prediction method for equilateral square and hexagonal facets as

$$\frac{L}{D} = K \sqrt{\frac{\delta_{\text{rms-pre}}}{D}} \frac{F}{D},\tag{10}$$

where *K* in Equation (10) is 6.160 for square facets and 4.046 for hexagonal facets. Equations (8) and (9) are widely used in stage of preliminary design of large DMRs to determine the maximum allowable facet size [14–16].

Meyer [17] introduced differential geometry of a mesh surface and used membrane theory to calculate RMS error for a mesh reflector. Fichter [18] extended theory in Equations (8)–(10) by considering stress of membrane within the facets. Similar with the work in Ref. [1], RMS error of a shallow reflector with equilateral triangular facets is predicted as

$$\frac{\delta_{\text{rms-pre}}}{D} = \frac{\sqrt{15}}{560} \frac{(L/D)^2}{F/D}.$$
 (11)

For equilateral rectangular facets of length 2h and width $2k = 2\rho h$, with $0 < \rho \le 1$, RMS error was estimated as

$$\frac{\delta_{\text{rms-pre}}}{D} = \frac{\sqrt{5}}{120} \sqrt{1 + \rho^4} \frac{(2h/D)^2}{F/D}.$$
 (12)

Hedgepeth [19, 20] considered mesh saddling in RMS error prediction by introducing stress of membrane within the facets, which was also pointed out in Refs. [13, 21]. When effect of membrane tension is considered, mesh of a reflector is often pulled into a dish shape by auxiliary chords attached to several interior points. The lateral loading tends to curve the supporting members inward. Thus, nodal positions of the mesh were suggested to be adjusted, so as to compensate this effect. According to Refs. [13, 19], RMS error of a mesh of equilateral triangular facets is estimated as

$$\frac{\delta_{\text{rms-pre}}}{D} = 0.01614 \frac{(L/D)^2}{F/D} \sqrt{1 + 0.660 \frac{pL}{t} + 0.133 \left(\frac{pL}{t}\right)^2},$$
(13)

where p and t are mesh tension and force in supporting elements.

Influences of member lengths imperfection and thermal strain on the surface accuracy of large DMRs were studied by many researchers in the past decades [5, 22–24]. RMS error prediction for various types of structures including tet-

rahedral truss, geodesic dome, radial ribs, and pretensioned truss were investigated by Hedgepeth [5]. For a geodesic dome, RMS error under member lengths imperfection is estimated as

$$\frac{\delta_{\text{rms-pre}}}{D} = \frac{2F}{D}\sigma_{\varepsilon},\tag{14}$$

where σ_{ε} is the standard deviation of member errors.

Hedgepeth [20] and Mobrem [25] used natural frequency results from available closed form solutions to estimate surface error under member length imperfection in preliminary design of a large DMR. In this inverse frequency squared method, weighted lump masses were assigned on nodes of a mesh in the direction normal to the reflecting surface. With computed natural frequencies w_i , RMS error is estimated by

$$\delta_{\text{rms-pre}} = \sqrt{\frac{\left(EAL\sigma_{\varepsilon}^{2}\right)_{\text{ref}}}{\bar{m}} \sum_{i=1}^{n} \frac{1}{w_{i}^{2}}},$$
(15)

where n is the number of modes, E and A are Young's modulus and the cross-sectional area of members, and \bar{m} is the total weighted masses. $(EAL\sigma_{\varepsilon}^2)_{\rm ref}$ is the reference values of these variables under the assumption of

$$EA_{i}L_{i}\sigma_{\varepsilon,i}^{2} = \left(EAL\sigma_{\varepsilon}^{2}\right)_{ref},$$
 (16)

where A_j , L_j , and $\sigma_{\varepsilon,j}^2$ are the cross-sectional area, length, and standard deviation of error of the *j*-th member.

RMS error prediction for mesh reflectors considering deformation caused by thermal loads during in-orbit missions was investigated in Ref. [5]. Due to a significant temperature change when entering or leaving the Earth's shadow, the corresponding thermal strain may result in large surface distortion of a mesh reflector. The work in Ref. [5] also studied temperature difference at nodes of a reflecting surface due to their different angles to solar radiation. RMS error was predicted in Equations (17) and (18) by the average strain $\varepsilon_{\rm ave}$ and the maximum shear strain $\gamma_{\rm max}$, if the strains are expressed in terms of equivalent biaxial membrane strains.

$$\frac{\delta_{\text{rms-pre}}}{D} = 0.0180 \frac{\varepsilon_{\text{ave}}}{F/D},\tag{17}$$

$$\frac{\delta_{\text{rms-pre}}}{D} = 0.0128 \frac{\gamma_{\text{max}}}{F/D}.$$
 (18)

The calculations of $\varepsilon_{\rm ave}$ and $\gamma_{\rm max}$ are given in Figure 13 of Ref. [5]

4. RMS Error Calculation for a Generated Mesh Geometry

Geometric surface error of a DMR can be obtained by either rough estimation (prediction) or analytical calculation. For a large DMR, rough surface error estimation (prediction), as introduced in Section 3, is only used for a preliminary design. When a mesh geometry is fully generated, evaluation

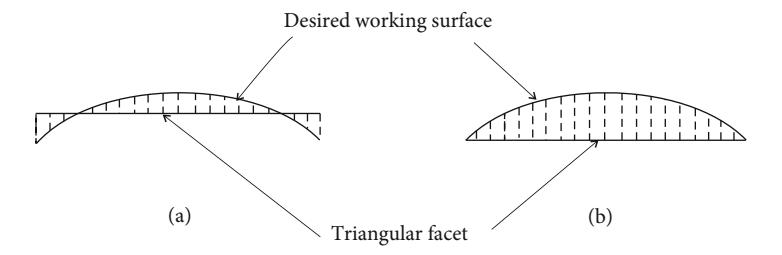


FIGURE 4: Triangular facet and desired working surface: (a) nodes are placed off the desired working surface and (b) nodes are placed on the desired working surface.

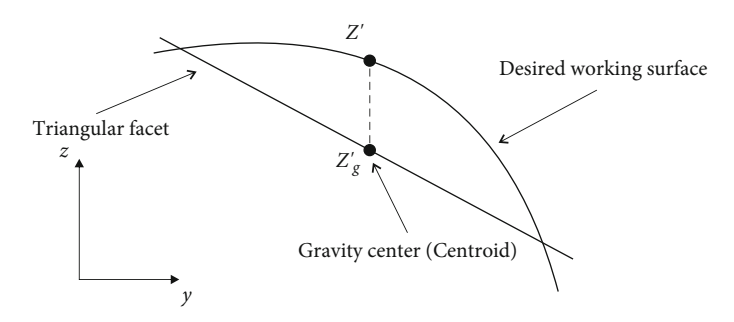


FIGURE 5: Geometric illustration of facet gravity center deviation RMS error.

of surface accuracy for a given topology and nodal positions are needed in complete DMR design, especially in comparing different structural design techniques [26] or form-finding methods [27, 28]. Methods of RMS error calculation for evaluating surface accuracy of a generated mesh geometry shall be introduced and compared in this section.

Surface accuracy of a generated mesh geometry in general can be evaluated by three methods: the nodal deviation RMS error, the best-fit surface RMS error, and the direct RMS error. Note that the nodal deviation RMS error and the best-fit surface RMS error do not measure a real deviation of the mesh geometry from the desired working surface. If stringent requirement on high surface accuracy in DMR design is implemented, or if nodes of a mesh geometry are placed off the desired working surface [29], the direct RMS error is necessary for a more accurate evaluation.

4.1. Nodal Deviation RMS Error. One commonly used evaluation of surface accuracy of a DMR is to calculate an RMS error due to deviation of the nodes of a mesh geometry from a desired working surface. For instance, such an RMS error $\delta_{\rm rms-n}$ can be expressed by [30, 31]

$$\delta_{\text{rms-n}} = \sqrt{\frac{1}{n} \sum_{i=1}^{n} \left(\Delta x_i^2 + \Delta y_i^2 + \Delta z_i^2 \right)}, \tag{19}$$

where Δx_i , Δy_i and Δz_i are the normal distances between the i-th node and the desired working surface in the x-, y- and z-directions and n is the total number of nodes. This method is developed under an assumption that the nodes of a reflector are moved off the desired working surface by certain predictable or unpredictable influences, such as thermal loads and

fabrication errors. While being simple and easy to use, the formula in Equation (19) is not accurate enough because it fails to consider geometric difference between facet planes and curved working surface. For instance, the surface deviation of a triangular facet from the desired working surface in Figure 4(a) should be smaller than that in Figure 4(b), but the $\delta_{\rm rms-n}$ in Equation (19) gives an opposite result simply because the facet nodes in Figure 4(a) are off the desired working surface. Furthermore, Equation (19) concludes zero surface error if all nodes of a mesh are on the desired working surface, regardless of the number of nodes, which is misleading.

Another type of nodal deviation RMS error, used in Ref. [32], is to compare values of two parameters: Z'_{g_i} and Z'_i , where Z'_{g_i} is the z-coordinate of the gravity center (centroid [1]) of the *i*-th computed triangular facet on the z-axis and Z'_i is the z-coordinate of the gravity center of the *i*-th computed triangular facet when projected vertically onto the desired working surface, shown in Figure 5. The RMS error $\delta_{\text{rms-gc}}$ is then given by

$$\delta_{\text{rms-gc}} = \left(\frac{\sum_{i=1}^{n} S'_{i} \left(Z'_{i} - Z'_{g_{i}}\right)^{2}}{\sum_{i=1}^{n} S'_{i}}\right)^{1/2}, \quad (20)$$

with S_i' being the projected area of the i-th triangular facet on the xy-plane. This calculation generally provides an evaluation of surface error with relatively low accuracy because only one point (gravity center) is used for each facet. This method is developed under an assumption that nodes of a triangular facet are placed on the desired working surface of a reflector. To achieve a more accurate evaluation of

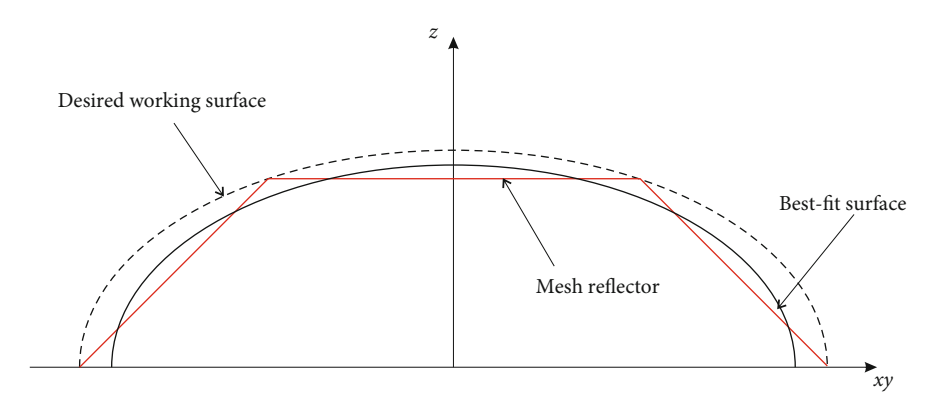


FIGURE 6: Schematic of the best-fit surface and desired working surface of a DMR.

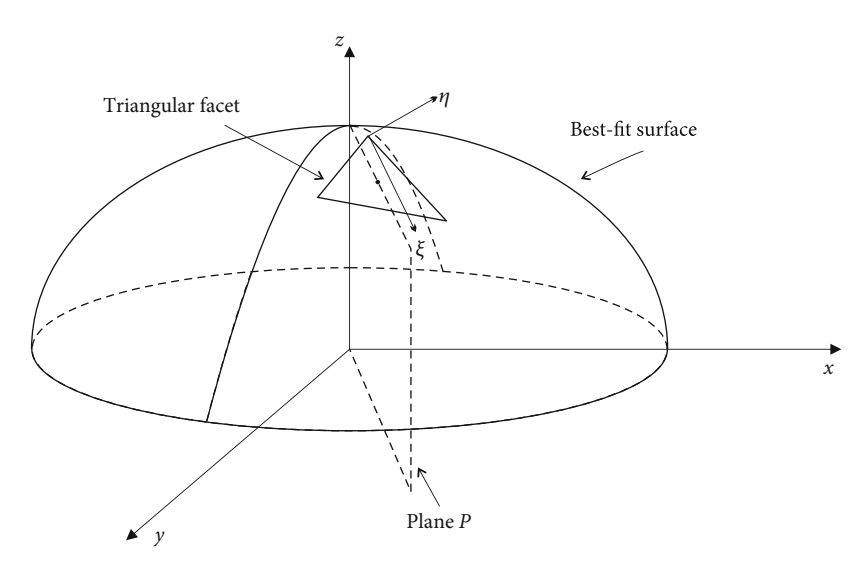


FIGURE 7: Local coordinate system (ξ, η) of a triangular facet in Ref. [1].

surface error, geometric difference between facet planes and desired working surface must be considered.

4.2. Best-Fit Surface RMS Error. After a mesh geometry of a DMR is generated, it is natural to find out what surface (spherical or parabolic) the mesh geometry best represents. A concept of best-fit surface is thus introduced. The best-fit surface of a DMR mesh geometry is a sphere or paraboloid, which, among all possible spherical or parabolic surfaces, has the least deviation from the mesh geometry [22, 33]. Such best-fit surface and the corresponding best-fit surface RMS error are obtained through a try and error process. To avoid confusion, the candidate of best-fit surface in each iteration is named effective surface [1]. For illustration, a schematic of a mesh geometry of a DMR, its best-fit surface, and the desired working surface is shown Figure 6.

The best-fit surface RMS error of a center-feed reflector is defined as follows. As shown in Figure 7, for a given triangular facet of the generated mesh, a plane P is defined by containing the z-axis and the centroid of the triangular facet. A local coordinate system (ξ, η) is generated by having a triangular facet node with the largest z-coordinate being

the origin. The ξ -axis is parallel to the intersection between plane P and plane of the triangular facet. The η -axis is in plane of the triangular facet, perpendicular to the ξ -axis. Let (ξ_1, η_1) , (ξ_2, η_2) , and (ξ_3, η_3) be positions of the three nodes of the triangular facet in the local coordinate system. Denote the normal distance between a point on the facet plane and the effective surface by ω (ξ, η) . The calculation of ω (ξ, η) was given in Ref. [1] with the mistakes corrected by Ref. [6] (see Equation (24)). By assuming a shallow desired working surface, an equation of ω is given as

$$\omega(\xi, \eta) = a + b\xi + c\eta + \frac{\xi^2}{2R_{\xi}} + \frac{\eta^2}{2R_{\eta}},$$
 (21)

where *a* is the normal distance from the three nodes of the triangular facet to the effective surface. Since the DMR is assumed to be shallow, the normal distances from the three nodes to the effective surface are the same in Equation (21).

In Equation (21), b and c are constants which shall be calculated later. R_{ξ} and R_{η} are radius of curvatures. For a spherical effective surface, $R_{\xi} = R_{\eta} = R$, where R is the radius of the sphere. For a parabolic effective surface,

$$R_{\xi} = 2F' \left[1 + \left(\frac{r_c}{2F'} \right)^2 \right]^{3/2},$$

$$R_{\eta} = r_c \sqrt{1 + \left(\frac{2F'}{r_c} \right)^2},$$
(22)

with $r_c = \sqrt{x_c^2 + y_c^2}$. x_c and y_c are the global coordinates of the centroid (gravity center) of the triangular facet. F' is the focal length of the effective surface. Assume the three nodes of the triangular facet are all on the effective surface (As shall be seen later in this section, it is almost impossible. This assumption is only for illustrative purpose.) and the origin of the local coordinate system (ξ, η) is at the first node of the facet, then obviously a=0 and $(\xi_1,\eta_1)=(0,0)$ and ω at the three nodes is

$$\omega(\xi_1, \eta_1) = \omega(0, 0) = 0,$$

 $\omega(\xi_2, \eta_2) = 0,$ (23)
 $\omega(\xi_3, \eta_3) = 0.$

Combining Equation (21) and Equation (23), the remaining constants are then obtained as

$$b = \frac{-(\eta_3 d_2 - \eta_2 d_3)}{4S},$$

$$c = \frac{(\xi_2 d_3 - \xi_3 d_2)}{4S},$$

$$S = \frac{1}{2} (\xi_2 \eta_3 - \xi_3 \eta_2),$$

$$d_i = \frac{\xi_i^2}{R_{\mathcal{E}}} + \frac{\eta_i^2}{R_n}.$$
(24)

S is the area of the triangular facet. It should be noticed that Equation (24) is different from (A. 5) in Ref. [1], which mistakenly calculated *b* as $b = (\eta_3 d_2 - \eta_2 d_3)/4S$.

With Equation (21), squared deviation of the facet plane from the effective surface is calculated by integrating ω^2 over the facet area S:

$$\phi = \iint_{S} \omega^2 d\xi d\eta = S \left| a^2 - \frac{af}{6} + \frac{f^2}{120} - \frac{S^2}{90R_{\xi}R_{\eta}} \right|, \quad (25)$$

where

$$f = \frac{\left(\xi_2^2 - \xi_2 \xi_3 + \xi_3^2\right)}{R_{\mathcal{E}}} + \frac{\left(\eta_2^2 - \eta_2 \eta_3 + \eta_3^2\right)}{R_n}.$$
 (26)

The effective surface RMS error $\delta_{\rm rms-eff}$ of the entire mesh then is defined by adding up ϕ of facets of the whole reflector and divided by the summation of facet areas, given

as follows:

$$\delta_{\text{rms-eff}} = \sqrt{\frac{1}{S_{\text{mesh}}} \sum_{i} \phi_{i}},$$
 (27)

where $S_{\text{mesh}} = \sum_{i} S_{i}$ is the total area of all facets of the mesh geometry.

The best-fit surface of a generated mesh geometry can then be found by properly determining its focal length $F_{\rm bf}$ and the vertex height $H_{\rm bf}$ through a try and error process, such that $\delta_{\rm rms-eff}$ in Equation (27) is minimized. Therefore, the value of a in each iteration is different. The calculation of a was given in Ref. [1] and the mistake which was corrected in Ref. [6].

Geometries of a general triangular mesh facet, a desired working surface, and an effective surface are given in Figure 8. The equations of the desired working surface and the effective surface are

$$x^2 + y^2 = 4F(H - x), (28)$$

$$x^{2} + y^{2} = 4F'(H - h - z),$$
 (29)

where h is distance in the vertical direction between the vertices of the desired working surface and the effective surface. H is height of the desired working surface. The facet plane is defined by an equation z = A + Bx + Cy.

There are two assumptions in the calculation of the bestfit RMS error: first, reflector is shallow; second, the nodes are all placed on the desired working surface. Thus, under the two assumptions, *a* is also the normal distance between the effective surface and the desired working surface for a given mesh facet.

A line \overline{PQ} is created by passing through the centroid C of the facet normal to its plane. The equation of the line in its plane created by r and z is given in (A. 10) of Ref. [1] which is represented here:

$$r^{2} = x^{2} + y^{2},$$

$$z = z_{c} + \frac{r - r_{c}}{\sqrt{B^{2} + C^{2}}},$$
(30)

where z_c and r_c are coordinates of the centroid of the facet. The r_c is given as

$$r_c^2 = x_c^2 + y_c^2. (31)$$

 r_p , r_q , z_p , and z_q are shown in Figure 8, and their formulas of calculation are obtained by substituting Equation (30) into Equations (28) and (29):

$$r_{q} = \frac{-2F}{\sqrt{B^{2} + C^{2}}} + 2\sqrt{\frac{F^{2}}{B^{2} + C^{2}}} + F\left(H - z_{c} + \frac{r_{c}}{\sqrt{B^{2} + C^{2}}}\right), \tag{32}$$

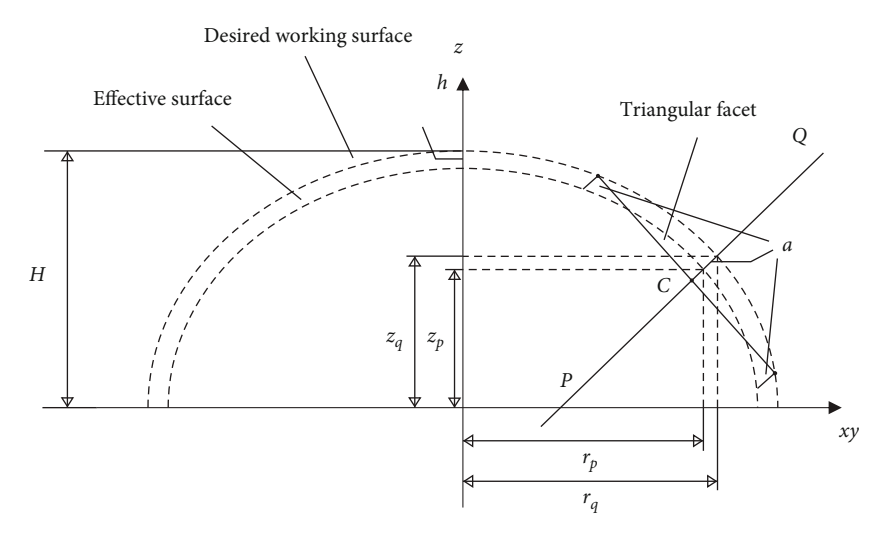


FIGURE 8: Geometries of desired working surface, effective surface, and a facet.

$$r_p = \frac{-2F'}{\sqrt{B^2 + C^2}} + 2\sqrt{\frac{F'^2}{B^2 + C^2} + F'\left(H - h - z_c + \frac{r_c}{\sqrt{B^2 + C^2}}\right)},$$
(33)

$$z_q = H - \frac{r_q^2}{4F},\tag{34}$$

$$z_p = H - h - \frac{r_p^2}{4F'},\tag{35}$$

$$a = \sqrt{(z_p - z_q)^2 + (r_p - r_q)^2},$$
 (36)

where Equation (35) is different from the incorrect form in (A. 12) of Ref. [1] shown in

$$z_p = H - \frac{r_q^2}{4F'}. (37)$$

With the value of a, the best-fit parabolic or sphere surface is then found by adjusting F' and h to minimize the RMS error in Equation (27). The optimal result is the best-fit surface RMS error $\delta_{\text{rms-bf}}$. This can be done by a numerical optimization algorithm [34].

$$\min \left[\delta_{\rm rms}\Big(F',h\Big)\right],\tag{38}$$

$$\begin{split} F_{bf} &= {F'}_{\min}, \\ H_{bf} &= H - h_{\min}. \end{split} \tag{39}$$

The evaluation of the best-fit surface of an offset-feed parabolic mesh geometry is different from that of a center-feed one and can be found in Ref. [6]. As shown in Figure 9, the parent paraboloid and its best-fit surface are in the global coordinates. Here, $D_{ca,bf}$ is the diameter of the circular aperture of the reflector's best-fit working surface which is the portion of the parent best-fit surface

within the offset aperture; $F_{p,bf}$ and $\Delta H_{g,bf}$ are the parent best-fit focal length and the vertical deviation; and φ is the slope of the best-fit parabola at the point intersecting with the parent aperture in the $x_g z_g$ -plane. From Figure 9,

$$D_{p,bf} = 4\sqrt{F_{p,bf}\left(H_g - \Delta H_{g,bf}\right)}, \tag{40}$$

$$\varphi = \sin^{-1}\left(\frac{D_{p,bf}}{2R_{s,bf}}\right),\tag{41}$$

$$\varphi_{off} = \tan^{-1} \left(\frac{H_g - e_z}{2R_c} \right). \tag{42}$$

If $\Delta H_{g,bf}$ is always sufficiently small, it can be assumed that

$$R_{s} = R_{s,bf},$$

$$\varphi = \varphi'.$$
(43)

From the geometry in Figure 9,

$$\frac{AC}{BC} = 1 - \frac{\tan(\varphi_{\text{off}})}{\tan(\varphi)}, \tag{44}$$

where

$$AC = \frac{1}{2} (D_{ca} - D_{ca,bf}),$$

$$BC = \frac{1}{2} (D_p - D_{p,bf}).$$
(45)

Hence,

$$D_{ca,bf} = D_{ca} - \frac{\tan(\varphi)}{\tan(\varphi) - \tan(\varphi_{\alpha\beta})} (D_p - D_{p,bf}). \tag{46}$$

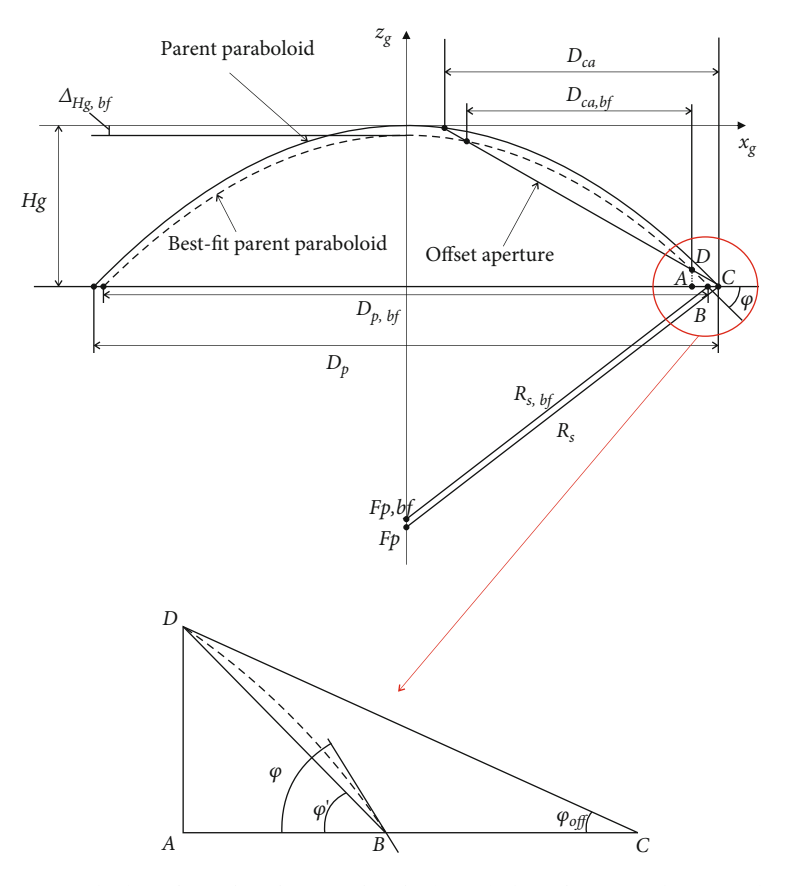


Figure 9: The best-fit surface for an offset-feed parabolic reflector in the $x_g z_g$ -plane.

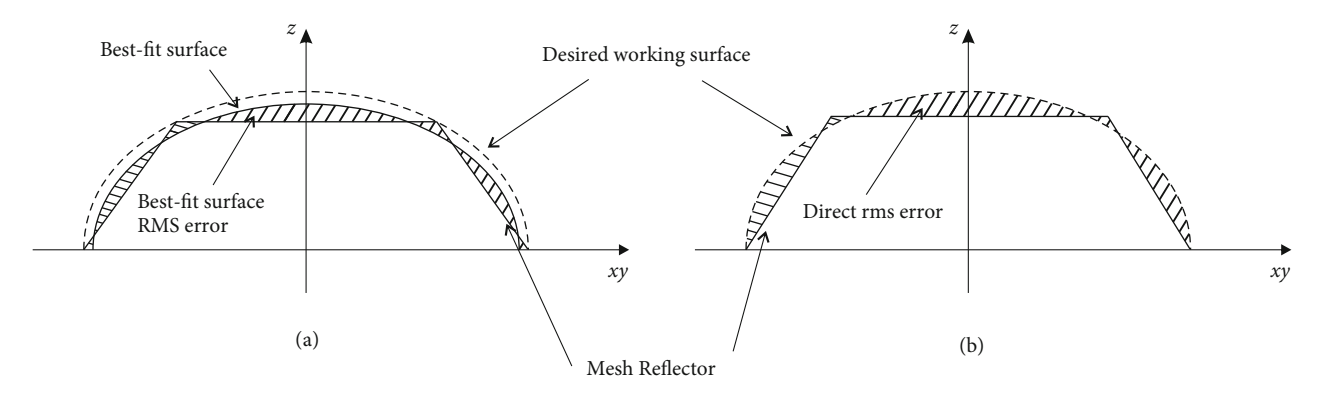


FIGURE 10: Comparison of two types of RMS errors: (a) the best-fit surface RMS error and (b) the direct RMS error.

4.3. Direct RMS Error. The best-fit surface RMS error described in Section 4.2 is not a true evaluation of geometric deviation of a DMR mesh geometry from its desired working surface. For design of a DMR with high surface accuracy, the direct RMS error that truly measures geometric deviation of a DMR mesh geometry from its desired working surface was proposed in Refs. [35, 36]. A comparison of these two types of RMS errors is shown in Figure 10.

Consider a typical triangular facet in Figure 11, where the desired working surface is also shown. To calculate the direct RMS error, a local coordinate system (τ, v) is estab-

lished on the facet plane; see Figure 12, where the origin can be any one of nodes of the facet. Let $\mu(\tau,v)$ be normal distance between a point on the facet plane and the desired working surface. Squared deviation of the triangular facet from the desired working surface is

$$\varphi = \iint_{S} \mu^2 d\tau dv. \tag{47}$$

By summing the deviations of all facets, the direct RMS error $\delta_{\rm rms-d}$ of a DMR mesh geometry is defined as follows:

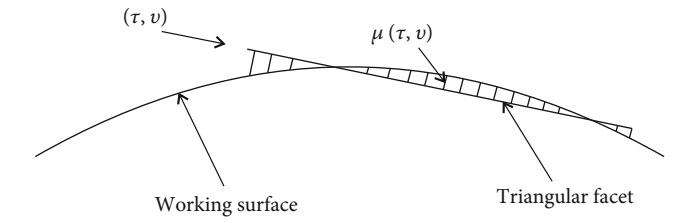


FIGURE 11: The desired working surface and a triangular facet for calculation of direct RMS error.

$$\delta_{\text{rms-d}} = \sqrt{\frac{1}{S_{\text{mesh}}} \sum_{i} \varphi_{i}}.$$
 (48)

Note that the distance ω (ξ, η) and the distance μ (τ, v) are not the same. In calculation of ω (ξ, η), many assumptions, including shallow reflecting surface and nodes being placed on the desired working surface, have been made. Because of this, formulas for computing the best-fit surface RMS error are not applicable in calculation of the direct RMS error. For example, normal distances from the three nodes of the triangular facets to the best-fit surface are assumed the same. This is not true in general case if stringent surface accuracy evaluation is required. For design of a DMR with high surface accuracy, exact analytical formulas for computing the direct RMS error are needed.

Equation (48) can be directly used to calculate the direct RMS error if μ is obtained. To obtain μ for a typical triangular facet, a local coordinate system (τ, v, μ) is defined in Figure 12, where the origin is at one of the facet nodes; the τ -axis is in the direction from (τ_1, v_1) to (τ_2, v_2) ; the v-axis is normal to the τ -axis, lying within the facet plane; and the μ -axis is normal to the facet plane. The equation of the facet plane in the global coordinate system (x, y, z) is

$$a_p x + b_p y + c_p z + d_p = 0,$$
 (49)

which can be obtained from coordinates of the three nodes, namely, (x_1,y_1,z_1) , (x_2,y_2,z_2) , and (x_3,y_3,z_3) . Here for convenience, it is assumed that the node (x_1,y_1,z_1) is the origin of the local coordinate system (τ,v,μ) . In the global coordinate system, let the unit vectors of the τ -, v-, and μ -axes be e_1 , e_2 , and e_3 , respectively. These unit vectors are given by

$$e_{1} = \frac{\left[x_{2} - x_{1} y_{2} - y_{1} z_{2} - z_{1}\right]^{T}}{\sqrt{\left(x_{2} - x_{1}\right)^{2} + \left(y_{2} - y_{1}\right)^{2} + \left(z_{2} - z_{1}\right)^{2}}},$$

$$e_{3} = \frac{1}{\sqrt{a_{p}^{2} + b_{p}^{2} + c_{p}^{2}}} \left[a_{p} b_{p} c_{p}\right]^{T},$$

$$e_{2} = \frac{e_{1} \times e_{3}}{\left|e_{1} \times e_{3}\right|}.$$
(50)

Denote the unit vectors of the global coordinate system xyz as e_1 ', e_2 ', and e_3 ', which are expressed by

$$e_{1}' = \begin{cases} 1 \\ 0 \\ 0 \end{cases},$$

$$e_{2}' = \begin{cases} 0 \\ 1 \\ 0 \end{cases},$$

$$e_{3}' = \begin{cases} 0 \\ 0 \\ 1 \end{cases}.$$
(51)

The coordinate transformation matrix E from the local coordinate system (τ, v, μ) to the global coordinated system (x, y, z) is given as

$$E = \begin{bmatrix} E_{11} & E_{12} & E_{13} \\ E_{21} & E_{22} & E_{23} \\ E_{31} & E_{32} & E_{33} \end{bmatrix} = \begin{bmatrix} e_1^T e_1' & e_1^T e_2' & e_1^T e_3' \\ e_2^T e_1' & e_2^T e_2' & e_2^T e_3' \\ e_3^T e_1' & e_3^T e_2' & e_3^T e_3' \end{bmatrix}.$$
(52)

The global and local coordinates are related by

Because E is an orthogonal matrix,

$$\left\{ \begin{array}{l} x \\ y \\ z \end{array} \right\} = E^{-1} \left\{ \begin{array}{l} \tau \\ v \\ \mu \end{array} \right\} + \left\{ \begin{array}{l} x_1 \\ y_1 \\ z_1 \end{array} \right\} = E^T \left\{ \begin{array}{l} \tau \\ v \\ \mu \end{array} \right\} + \left\{ \begin{array}{l} x_1 \\ y_1 \\ z_1 \end{array} \right\}.$$

$$(54)$$

It follows that the global coordinates can be expressed by

$$x = E_{11}\tau + E_{21}v + E_{31}\mu + x_1,$$

$$y = E_{12}\tau + E_{22}v + E_{32}\mu + y_1,$$

$$z = E_{13}\tau + E_{23}v + E_{33}\mu + z_1.$$
(55)

Recall that the equation of the desired parabolic working surface is

$$z - H = -\frac{1}{4F} \left(x^2 + y^2 \right). \tag{56}$$

Substitute Equation (55) into Equation (56) and rearrange the resulting equation with respect to μ to obtain

$$a_1\mu^2 + a_2\mu + a_3 = 0, (57)$$

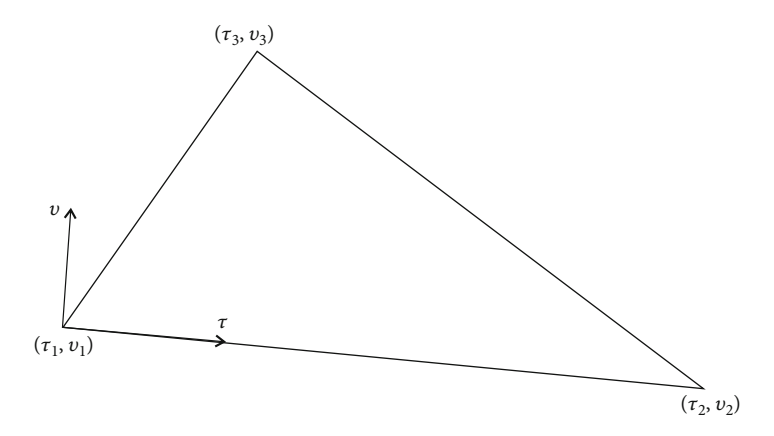


FIGURE 12: Local coordinate of a triangular facet for calculation of direct RMS error.

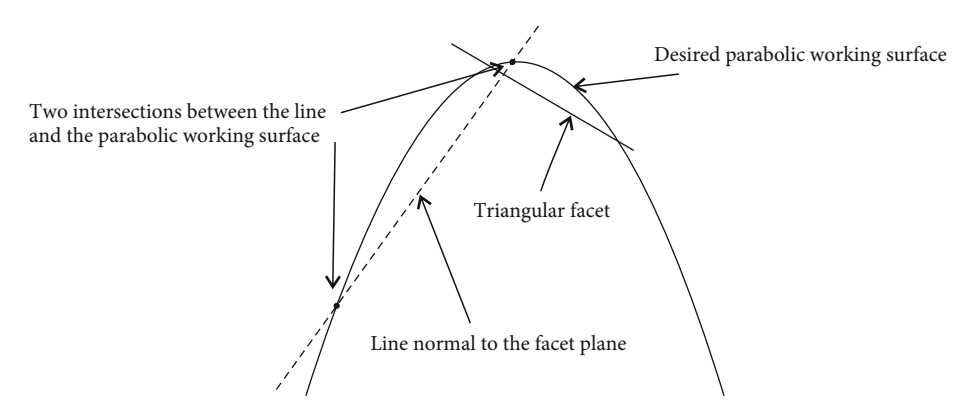


FIGURE 13: Two intersections between the line normal to the facet plane and the desired parabolic working surface.

with

$$\begin{split} a_1 &= \left(E_{31}^2 + E_{32}^2\right)\frac{1}{4F},\\ a_2 &= E_{33} + E_{31}(x_1 + E_{11}\tau + E_{21}\upsilon)\frac{1}{2F} + E_{32}(y_1 + E_{12}\tau + E_{22}\upsilon)\frac{1}{2F},\\ a_3 &= -H + z_1 + E_{13}\tau + E_{23}\upsilon + \left(x_1 + E_{11}\tau + E_{21}\upsilon\right)^2\frac{1}{4F} + \left(y_1 + E_{12}\tau + E_{22}\upsilon\right)^2\frac{1}{4F}. \end{split}$$
 (58)

According to Equation (57), μ is a function of τ and v, namely, $\mu = \mu(\tau, v)$. For a point (τ^*, v^*) on the facet, $\mu(\tau^*, v^*)$ is the normal distance from the point on the facet to the parabola as described by Equation (56). Solution of Equation (57) gives

$$\mu(\tau, v) = \frac{-a_2 \pm \sqrt{a_2^2 - 4a_1 a_3}}{2a_1}.$$
 (59)

As shown in Figure 13, for a line that is normal to the facet plane and passes through one point on the facet, there are two intersections between the line and the parabola. For calculation of the direct RMS error, only the intersection with smaller distance from the point on the facet represents the deviation of the point from the desired working surface. Thus, out of the two roots given by Equation (59), only the one with smaller abso-

lute value is the true solution. With such selected μ , the direct RMS error can be computed by Equations (47) and (48).

Note that the double integral in Equation (47) can also be computed numerically by applying the coordinate transformation technique introduced in Equations (49)–(59). This calculation is efficient especially when number of facets of a reflecting surface is large.

In this section, the nodal deviation RMS error, the bestfit surface RMS error, and the direct RMS error for surface accuracy evaluation of a generated mesh geometry are reviewed. The reviewed RMS calculation methods are compared in Table 1 in terms of computational efficiency and working requirements.

5. Effective Region RMS Error

During in-orbit mission of a large DMR, only central portion of the reflecting surface is being used for signal transmission since accuracy of boundary layers of the reflector is usually low. This portion of a DMR is called effective region. It is desired in design of a DMR to obtain a large effective region area. However, many DMR designs can only deliver a reflecting surface either with high surface accuracy and small effective region area, or with low surface accuracy and large effective region area. Therefore, calculation of RMS error also calls for consideration of the effective region area.

	Nodal deviation	Facet gravity center deviation	Best-fit surface	Direct RMS
	RMS error $\delta_{\mathrm{rms-n}}$	RMS error $\delta_{ m rms-gc}$	RMS error $\delta_{ m rms-bf}$	error $\delta_{ m rms-d}$
Computational efficiency	High	High	Low	Low
Nodes placed on the working surface	Not allowed	Required	Required	Not required
Nodes placed off the working surface	Required	Not allowed	Not allowed	Not required
Shallow working surface	Not required	Not required	Required	Not required

Table 1: Comparison of RMS error calculation methods for surface accuracy evaluation of a mesh geometry.

For convenience of analysis and design, working surface of a DMR can be viewed as a cluster of cocentered facet layers, as shown Figure 14, where each layer is a ring of facets. The layers are assigned index numbers starting from the center of the working surface, with the first layer consisting of the center of the reflector and the last layer being the one connected to the boundary. Accordingly, a layer of a smaller index number is closer to the center of the working surface than a layer of a larger index number.

A definition of effective region of a DMR was carried out by Yuan et al. [37]. In this definition, the effective region was considered as a portion of its working surface that meets the surface accuracy requirement for signal transmission. For a smooth working surface (either parabolic or spherical), due to the vertical directions of tension tie forces, the slope of a point on the surface that is near the boundary is larger than that of a point which is relatively away from the boundary. Because of this, for an almost uniform distribution of cable member tensions, a layer of a smaller index number has shorter member lengths than a layer of a larger index number [6]. This yields smaller RMS errors for the inner layers of a reflector. Thus, the layers of a working surface can be divided into two types: (i) the inner layers, which are closer to the center of the working surface and meet the surface accuracy requirement, and (ii) the outer layers, which are near the boundary of the working surface and do not satisfy the surface accuracy requirement. Obviously, the effective region of a DMR is formed by all the inner layers.

Assume that the working surface of a designed DMR has n_r facet layers. Let the RMS error of the k-th layer be $\delta_{\rm rms,k}$, $k=1,2,\cdots,n_r$, which can be easily computed [38]. Assume that the reflector working surface has k_{er} inner layers. According to the above discussion, the effective region of the DMR is formed by the first $k_{\rm er}$ layers of the working surface. In other words, $\delta_{\rm rms,k} \leq \delta_{\rm rms}$ for $1 \leq k \leq k_{\rm er}$ and $\delta_{\rm rms,k} > \delta_{\rm rms}$ for $k_{\rm er} + 1 \leq k \leq n_r$, where $\delta_{\rm rms}$ is the required surface error upper bound given in Equation (5).

One objective in design of a DMR is to assure enough effective region area for operation. For a reflector, which can be either a center-feed parabolic reflector or an offset-feed parabolic reflector, its effective region can be calculated by $S_e = \sum_{k=1}^{k_{er}} S_k$ where S_k is the surface area of the k-th layer. The RMS error $\delta_{\rm rms-er}$ of the effective region can be evaluated either by the outmost inner layer:

$$\delta_{\text{rms-er}} = \frac{\delta_{\text{rms},k_{er}}}{\beta},\tag{60}$$

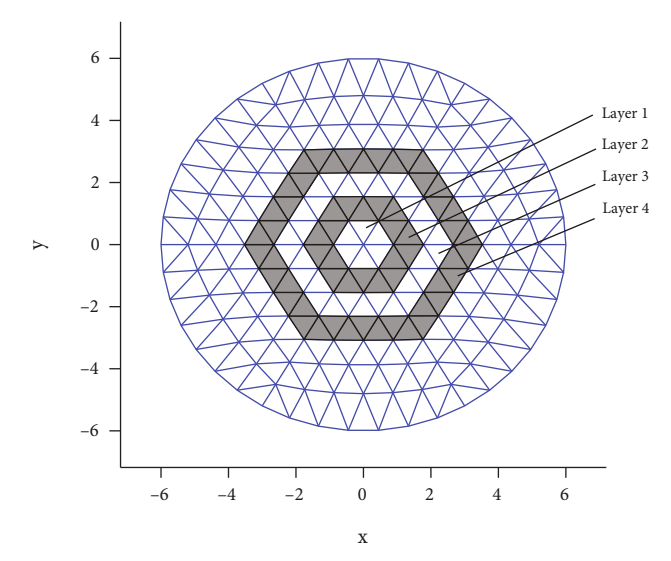


FIGURE 14: Layers of a mesh geometry of a DMR.

or by a mean value:

$$\delta_{\text{rms-er}} = \frac{1}{S_e \beta} \sum_{k=1}^{k_{er}} S_k \delta_{\text{rms},k}, \tag{61}$$

where

$$\beta = \frac{S_e}{S},\tag{62}$$

with *S* being the area of the whole aperture of the reflector. Note that for a reflector without a clear aperture rim, for example, some reflectors are hexagonal with only six nodes being attached to a supporting structure [15], *S* in Equation (62) is the area of all mesh facets that are used for reflecting signals.

6. Numerical Examples

In this work, several methods of RMS error calculation for large DMRs have been reviewed. For a clearly comparison, the nodal deviation RMS errors, the best-fit surface RMS errors, and the direct RMS errors of three mesh geometries (a two-facet mesh geometry, a center-feed parabolic DMR, and an offset-feed parabolic DMR) are calculated, respectively. Advantages and limitations of the reviewed methods of RMS error calculation shall be presented by examples in this section.

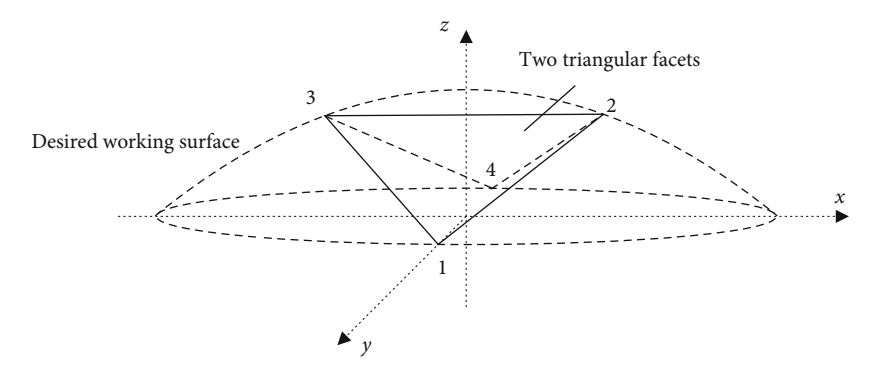


FIGURE 15: Two triangular facets with nodes being placed on the desired working surface.

6.1. A Two-Facet Mesh Geometry

6.1.1. Calculation of the Nodal Deviation RMS Error. A two-facet mesh geometry and a desired working surface are shown in Figure 15. Recall the two assumptions (shallow desired working surface and placement of nodes on the desired working surface) made in the best-fit RMS error calculation; the desired working surface in this example is a shallow center feed parabola with focal length F being 10 meters and aperture diameter D being 4 meters. Equation of the desired working surface is

$$z - 0.1 = -\frac{1}{40} (x^2 + y^2). \tag{63}$$

The four nodes that form the two triangular facets are placed on the desired working surface, with coordinates given as

$$(x_1, y_1, z_1) = (0, -2, 0),$$

 $(x_2, y_2, z_2) = (1, 0, 0.075),$
 $(x_3, y_3, z_3) = (-1, 0, 0.075),$
 $(x_4, y_4, z_4) = (0, 2, 0).$
(64)

Thus, the gravity center of the two facets are

$$(x_{c,1}, y_{c,1}, z_{c,1}) = (0, -0.6667, 0.05),$$

$$(x_{c,2}, y_{c,2}, z_{c,2}) = (0, 0.6667, 0.05).$$
(65)

For the nodal deviation RMS error calculated in Equation (19), calculation is trivial with $\delta_{\rm rms-n}=0$, because all nodes of the mesh geometry are on the desired working surface. Calculation in Equation (20) is given as

$$\delta_{\text{rms-gc}} = \left(\frac{\sum_{t=1}^{n} S'_{t} \left(Z'_{t} - Z'_{g_{t}}\right)^{2}}{\sum_{t=1}^{n} S'_{t}}\right)^{1/2} = 0.0389, \quad (66)$$

with

$$S'_{1} = 2,$$
 $S'_{2} = 2,$
 $Z'_{1} = 0.0889,$
 $Z'_{2} = 0.0889,$
 $Z'_{g_{1}} = 0.05,$
 $Z'_{g_{2}} = 0.05.$
(67)

6.1.2. Calculation of the Best-Fit Surface RMS Error. The best-fit surface RMS error is obtained by properly determining a best-fit surface of a mesh geometry through an iterative process that is usually solved by a numerical optimization algorithm [34]. To show application of the technique, calculation of the best-fit surface RMS error in one iteration is given in details. In this iteration, focal length F' of the effective surface and the vertices distance h between the effective surface and the desired working surface are assumed as 9.9 meters and 0.01 meter, respectively.

The first step is to define two local coordinate systems (ξ , η) for the two triangular facets and obtain local coordinates for nodes of the two facets as

$$\xi_{1,1} = 0,$$

$$\xi_{1,2} = 2.0014,$$

$$\xi_{1,3} = 0,$$

$$\xi_{2,1} = 0,$$

$$\xi_{2,2} = 0,$$

$$\xi_{2,3} = 2.0014,$$

$$\eta_{1,1} = 0,$$

$$\eta_{1,2} = -1,$$

$$\eta_{1,3} = -2,$$

$$\eta_{2,1} = 0,$$

$$\eta_{2,2} = 2,$$

$$\eta_{2,3} = 1.$$
(68)

 $\label{thm:thm:comparison} T_{ABLE} \; 2: \; Comparison \; of \; different \; RMS \; error \; calculation \; methods \; (mm).$

	Nodal deviation RMS error $\delta_{ m rms-n}$	Facet gravity center deviation RMS error $\delta_{ m rms-gc}$	Best-fit surface RMS error $\delta_{ m rms-bf}$	Direct RMS error $\delta_{\mathrm{rms-d}}$
Mesh geometry with two facets	0	38.9	7.7	30.2

Areas S of the two facets are

$$S_1 = S_2 = 2.0014. (69)$$

 ϕ_1 and ϕ_2 are calculated as

$$\phi_1 = \phi_2 = \iint_S \omega^2 d\xi d\eta = 8.6921 \times 10^{-4}.$$
 (70)

The RMS error of this effective surface is

$$\delta_{\text{rms-eff}} = \sqrt{\frac{1}{S_{\text{mesh}}} \sum_{i} \phi_{i}} = 0.0208. \tag{71}$$

According to the definition of the best-fit surface RMS error, in a numerical optimization algorithm, $\delta_{\rm rms-eff}$ is calculated in each iteration with F' and h being adjusted until the smallest value of $\delta_{\rm rms-eff}$ is found. This value is the best-fit RMS error $\delta_{\rm rms-bf}$. After minimized by the numerical optimization algorithm, the best-fit RMS error is obtained as

$$\delta_{\text{rms-bf}} = 0.0077, \tag{72}$$

with the corresponding $F_{\rm bf}$ and $h_{\rm bf}$ being 10 meters and 0.0292 meter. Thus, equation of the best-fit surface is

$$z - 0.0708 = -\frac{1}{40} (x^2 + y^2). \tag{73}$$

6.1.3. Calculation of the Direct RMS Error. For direct RMS error calculation, nodal coordinates of the two facets under local coordinate system (τ, v) are

$$\tau_{1,1} = 0$$

$$\tau_{1,2} = 2.2373$$

$$\tau_{1,3} = 0$$

$$\tau_{2,1} = 0,$$

$$\tau_{2,2} = 2,$$

$$\tau_{2,3} = 1,$$

$$v_{1,1} = 0,$$

$$v_{1,2} = 1.3434,$$

$$v_{1,3} = 1.7891,$$

$$v_{2,1} = 0,$$

$$v_{2,2} = 0,$$

$$v_{2,3} = -2.0014.$$
(74)

Due the simplicity of this example, φ for the two facets

can be directly obtained as

$$\varphi_1 = \varphi_2 = \iint_{S_1} \mu_1^2 d\tau dv = 1.8193 \times 10^{-3}.$$
 (75)

The direct RMS error is then calculated as

$$\delta_{\text{rms-d}} = \sqrt{\frac{1}{S_{\text{mesh}}} \sum_{i} \varphi_{i}} = 0.0302.$$
 (76)

For comparison, the RMS errors calculated by the three methods reviewed are listed in Table 2.

6.2. A Center-Feed Mesh Reflector and an Offset-Feed Mesh Reflector. In this section, the reviewed methods of RMS error calculation shall be applied to a parabolic center-feed mesh reflector and a parabolic offset-feed mesh reflector both with 127 nodes. The aperture diameter D of the center-feed reflector is 12 meters, with the focal ratio (F/D) being 0.5. F is the focal length of the center-feed reflector. The aperture diameter D_p of the parent parabola of the offset-feed reflector is 12 meters, with the focal ratio (F_p/D_p) being 0.33. F_p is the focal length of the parent parabola of the offset-feed reflector. The offset distance is 1 meter. Technique of boundary nodes reduction introduced in Ref. [6] is applied to topology design of both reflectors. Form findings of these reflectors are done by the fixed nodal position method introduced in Ref. [28]. For simplicity, all nodes are placed on the desired working surfaces. Top views of these two reflectors that show topology designs and effective region areas are given in Figure 16.

The nodal deviation RMS error $\delta_{
m rms-n}$, the facet gravity center deviation RMS error δ_{rms-gc} , the best-fit surface RMS error $\delta_{\rm rms-bf}$, the direct RMS error $\delta_{\rm rms-d}$, and the effective region RMS error δ_{rms-d} of this mesh reflector are listed in Table 3. From observation of Table 3, RMS errors vary significantly in different calculation methods. Methods that only consider nodal deviation have limitation for stringent surface accuracy analysis because it fails to consider geometric difference between the facet planes and the curved desired working surface. The best-fit surface RMS error, while being used in many cases, measures deviation of a mesh geometry from its best-fit surface, not the desired working surface. This is an accurate evaluation only for shallow reflectors with nodes all being placed on the desired working surface. When a reflector is deep or nodes are placed off the desired working surface, the best-fit surface RMS error is not an appropriate measurement. Since the best-fit surface so generated is different from the desired working surface, the location of focal point of the reflector also changes. So the best-fit surface RMS error does not applied to a DMR with fixed feed source. The direct RMS

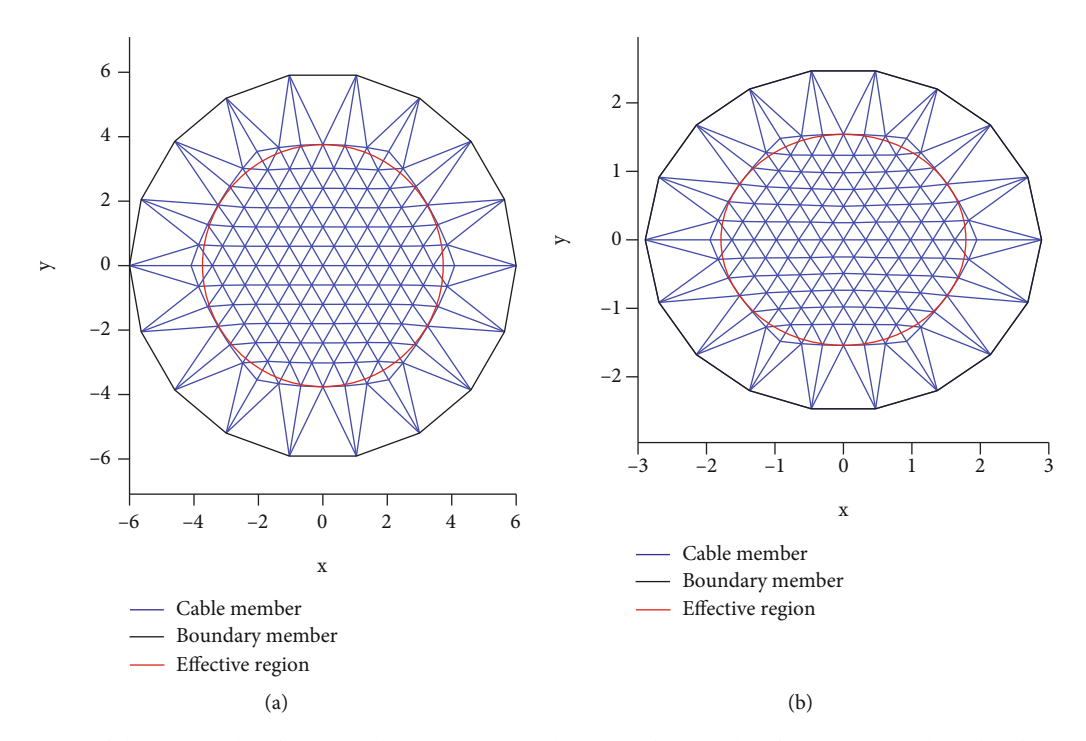


FIGURE 16: Top view of the two mesh reflectors with 127 nodes: (a) the center-feed mesh reflector and (b) the offset-feed mesh reflector.

Table 3: Comparison of different RMS error calculation methods (mm).

	Nodal deviation RMS error δ_{rms-n}	Facet gravity center deviation RMS error $\delta_{ m rms-gc}$	Best-fit surface RMS error $\delta_{ m rms-bf}$	Direct RMS error $\delta_{\rm rms-d}$	Effective region RMS error $\delta_{ m rms-er}$
Center-feed mesh reflector	0	7.08	1.40	4.24	10.22
Offset-feed mesh reflector	0	2.41	0.44	1.26	3.50

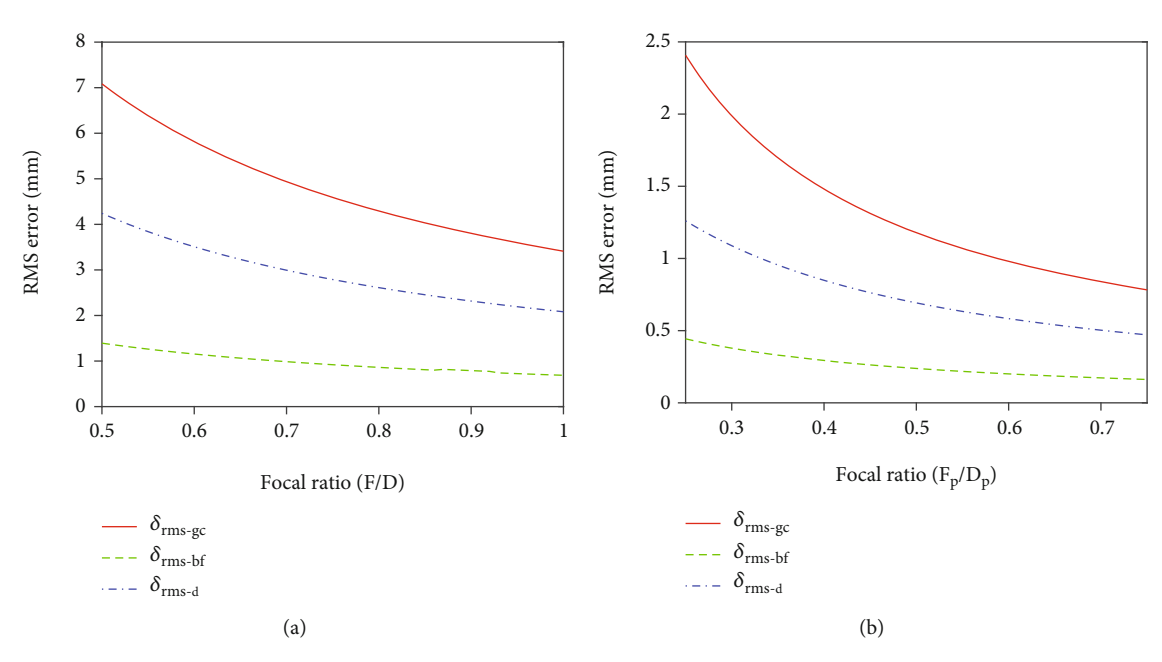


FIGURE 17: Comparison of RMS errors as the focal ratio increases for (a) the center-feed mesh reflector and (b) the offset-feed mesh reflector.

error evaluates deviation of a mesh geometry directly from the desired working surface. It is extremely useful in evaluating a reflector with high surface accuracy requirement. It is applicable to both shallow and deep reflectors, while allowing nodes being placed both on and off the desired working surface. It can also be observed from Table 3 that the $\delta_{\rm rms-er}$

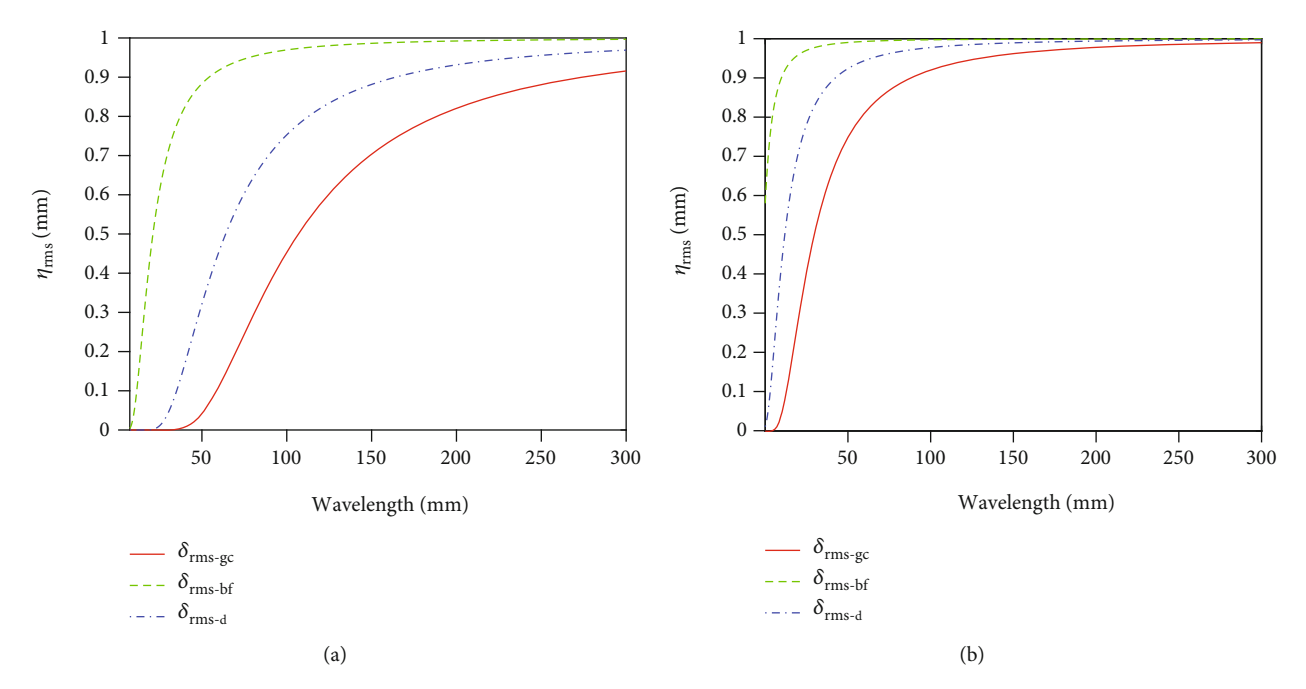


FIGURE 18: Comparison of reflector gain efficiency factor η_{rms} obtained by the three RMS error calculation methods, δ_{rms-gc} , δ_{rms-bf} , and δ_{rms-d} for (a) the center-feed mesh reflector and (b) the offset-feed mesh reflector.

is not always consistent with other definitions of RMS errors, since the effective region area is also included in the surface accuracy evaluation. For a reflector with smaller effective region area, $\delta_{\rm rms-er}$ can still be large even when the RMS error of facets within the effective region is small.

In addition, the simulation results show that that the RMS errors of the offset-feed mesh reflector are much smaller than those of the center-feed mesh reflector. This is because an offset-feed mesh reflector is cut from a parent sphere or parabola. Thus, it is usually shallower than a center-feed reflector with a similar aperture diameter. As seen in many reflector designs, a shallow DMR can achieve a much higher surface accuracy than a deep one.

The comparison of the three RMS error calculation methods, $\delta_{\rm rms-gc}$, $\delta_{\rm rms-bf}$, and $\delta_{\rm rms-d}$, under different focal ratio are presented in Figure 17. As seen in the simulation results, all the three RMS errors decrease as the focal ration of the reflector increases, because a shallow DMR with high focal ratio can achieve a much higher surface accuracy than a deep one with low focal ratio. This property is successfully captured by all the three methods in comparison.

The comparison of the reflector gain efficiency factor $\eta_{\rm rms}$ in Equation (6) under the three RMS error calculation methods, $\delta_{\rm rms-gc}$, $\delta_{\rm rms-bf}$, and $\delta_{\rm rms-d}$ within a wavelength range of 7.5-300 mm are plotted in Figure 18. As seen in Figure 18, differences among the reflector gain/loss estimations by the three methods of RMS error calculation are significant. Meanwhile, the reflector gain efficiency factor $\eta_{\rm rms}$ varies for different wavelengths. Note that Equation (6) is only for rough estimation of RMS error impact on the reflector gain. Accurate reflector gain evaluation requires a detailed radiofrequency analysis, which can be performed by a software for radiofrequency pattern calculation.

7. Conclusions

Methods of root-mean-square error calculation for large deployable mesh reflectors are reviewed. The main results from this investigation are summarized as follows.

- (i) Concept of reflector gain and effective surface error (half path length error) are given. The reflector gain is a factor to measure the reflector performance
- (ii) Approaches to RMS error prediction or estimation in preliminary design of large deployable mesh reflectors are shown. The predicted RMS error can be used as a guidance in reflector design, mainly to determine the maximum allowable member length. Influences of mesh saddling, thermal loads, and member length imperfection are considered in these estimations
- (iii) Methods of RMS error calculation for generated mesh geometry of large deployable mesh reflectors are presented. The nodal deviation RMS error is easy to implement but fails to include geometric difference between facet planes and the desired working surface. The best-fit surface RMS error evaluates deviation of a mesh geometry from its best-fit surface. This method requires shallow reflector and nodes being placed on the desired working surface. Therefore, the best-fit surface RMS error is not applicable to mesh reflectors with stringent surface accuracy requirement. In addition, the best-fit surface RMS error cannot be used to evaluate surface accuracy for a mesh geometry with nodes being placed off the desired working surface. The direct RMS error calculates deviation of a mesh geometry

- directly from the desired working surface. It is applicable to both shallow and deep reflecting surfaces. It also allows reflector nodes to be placed off the desired working surface. For complicated mesh geometry with many facets, numerical methods may be required in calculating the double integral of normal distance between the facets to the desired working surface over the facet area
- (iv) Concept of effective region is introduced. An adjusted measurement of surface accuracy is suggested when the concept of effective region is involved. This measurement has two evaluation factors, the effective region area and the RMS error of facets within the effective region
- (v) RMS errors of a mesh geometry with two triangular facets, a center-feed mesh reflector, and an offsetfeed mesh reflector are calculated by the RMS error calculation methods reviewed. Results in these demonstrative examples show that RMS errors may vary significantly if calculated by different methods
- (vi) The effective region RMS error is also used in measuring surface accuracy for a center-feed mesh reflector and an offset-feed mesh reflector. Numerical results show importance and necessity of considering the area of effective region in surface accuracy evaluation of large deployable mesh reflectors

Conflicts of Interest

The author declares no conflicts of interest.

Acknowledgments

The author acknowledges support from the US NSF (National Science Foundation) through grant 2104237.

References

- [1] P. K. Agrawal, M. S. Anderson, and M. F. Card, "Preliminary design of large reflectors with flat facets," *IEEE Transactions on Antennas and Propagation*, vol. 29, no. 4, pp. 688–694, 1981.
- [2] R. Nie, B. He, and L. Zhang, "Deployment dynamics modeling and analysis for mesh reflector antennas considering the motion feasibility," *Nonlinear Dynamics*, vol. 91, no. 1, pp. 549–564, 2018.
- [3] Y. Tang, T. Li, and X. Ma, "Pillow distortion analysis for a space mesh reflector antenna," *AIAA Journal*, vol. 55, no. 9, pp. 3206–3213, 2017.
- [4] S. Yuan, B. Yang, and H. Fang, "Enhancement of large deployable mesh reflectors by the self-standing truss with hardpoints," in *In: AIAA Scitech 2019 Forum*, Session: Spacecraft Antennas, and Other Optical Apertures, p. 752, San Diego, California, 2019.
- [5] J. M. Hedgepeth, "Accuracy potentials for large space antenna reflectors with passive structure," *Journal of Spacecraft and Rockets*, vol. 19, no. 3, pp. 211–217, 1982.

- [6] H. Shi, S. Yuan, and B. Yang, "New methodology of surface mesh geometry design for deployable mesh reflectors," *Journal of Spacecraft and Rockets*, vol. 55, no. 2, pp. 266–281, 2018.
- [7] J. Ruze, "Antenna tolerance theory—a review," *Proceedings of the IEEE*, vol. 54, no. 4, pp. 633–640, 1966.
- [8] H. Tanaka, "Surface error estimation and correction of a space antenna based on antenna gainanalyses," *Acta Astronautica*, vol. 68, no. 7-8, pp. 1062–1069, 2011.
- [9] R. Spencer, "A least square analysis of the effect of phase errors on antenna gain, Air Force Cambridge Research Laboratories," *Ref. E*, vol. 5025, p. 1949, 1949.
- [10] M. Zarghamee, "On antenna tolerance theory," *IEEE Transactions on Antennas and Propagation*, vol. 15, no. 6, pp. 777–781, 1967.
- [11] C. Jenkins, J. Wilkes, and D. Marker, "Improved surface accuracy of precision membrane reflectors through adaptive rim control," in *In: 39th AIAA/ASME/ASCE/AHS/ASC Structures, Structural Dynamics, and Materials Conference and Exhibit*, p. 1983, Long Beach, CA, U.S.A., 1998.
- [12] A. Miyasaka, M. Homma, A. Tsujigata, K. Nakamura, K. Yamada, and A. Meguro, "Design and ground verification of large deployable reflector," in *In: 19th AIAA Applied Aerodynamics Conference*, p. 1480, Anaheim, CA, U.S.A., 2001.
- [13] G. Tibert, Deployable Tensegrity Structures for Space Applications[Ph.D. thesis], KTH, Stockholm, Sweden, 2002.
- [14] M. Thomson, "AstroMesh deployable reflectors for ku and ka band commercial satellites," in *In: 20th AIAA International Communication Satellite Systems Conference and Exhibit*, p. 2032, Montreal, Quebec, Canada, 2002.
- [15] A. Tibert and S. Pellegrino, "Deployable tensegrity reflectors for small satellites," *Journal of Spacecraft and Rockets*, vol. 39, no. 5, pp. 701–709, 2002.
- [16] Y. Tang, T. Li, Z. Wang, and H. Deng, "Surface accuracy analysis of large deployable antennas," *Acta Astronautica*, vol. 104, no. 1, pp. 125–133, 2014.
- [17] R. X. Meyer, "Precision of mesh-type reflectors for large spaceborne antennas," *Journal of Spacecraft and Rockets*, vol. 22, no. 1, pp. 80–84, 1985.
- [18] W. Fichter, "Reduction of root-mean-square error in faceted space antennas," AIAA Journal, vol. 22, no. 11, pp. 1679– 1684, 1984.
- [19] J. M. Hedgepeth, Accuracy Potentials for Large Space Antenna Structures, Astro Research Corporation Carpinteria, California, United States, 1980.
- [20] J. M. Hedgepeth, "Influence of fabrication tolerances on the surface accuracy of largeantenna structures," *AIAA Journal*, vol. 20, no. 5, pp. 680–686, 1982.
- [21] K. Miura and K. Tanizawa, "Tension truss antenna—concept, reality and future," in *In: IUTAM-IASS Symposium on Deployable Structures: Theory and Applications*, pp. 291–300, Springer, Cambridge, UK, 2000.
- [22] W. H. Greene, "Effects of random member length errors on the accuracy and internal loads of truss antennas," *Journal of Spacecraft and Rockets*, vol. 22, no. 5, pp. 554–559, 1985.
- [23] Y. Zong, N. Hu, B. Duan, G. Yang, H. Cao, and W. Xu, "Manufacturing error sensitivity analysis and optimal design method of cable-network antenna structures," *Acta Astronautica*, vol. 120, pp. 182–191, 2016.
- [24] H. Shi, B. Yang, M. Thomson, and H. Fang, "Coupled elasticthermal dynamics of deployable mesh reflectors," in *In: 52nd*

- AIAA/ASME/ASCE/AHS/ASC Structures, Structural Dynamics and Materials Conference, p. 2001, Denver, Colorado, 2011.
- [25] M. Mobrem, "Methods of analyzing surface accuracy of large antenna structures due to manufacturing tolerances," in *In:* 44th AIAA/ASME/ASCE/AHS/ASC Structures, Structural Dynamics, and Materials Conference, AIAA, p. 1453, Norfolk, Virginia, 2003.
- [26] R. Nie, B. He, L. Zhang, and Y. Fang, "Deployment analysis for space cable net structures with varying topologies and parameters," *Aerospace Science and Technology*, vol. 68, pp. 1–10, 2017.
- [27] R. Nie, B. He, D. H. Hodges, and X. Ma, "Form finding and design optimization of cable network structures with flexible frames," *Computers & Structures*, vol. 220, pp. 81–91, 2019.
- [28] S. Yuan and B. Yang, "The fixed nodal position method for form finding of high-precision lightweight truss structures," *International Journal of Solids and Structures*, vol. 161, pp. 82–95, 2019.
- [29] S. Yuan, B. Yang, and H. Fang, "Improvement of surface accuracy for large deployable mesh reflectors," in *In: AIAA/AAS Astrodynamics Specialist Conference*, AIAA, p. 5571, Long Beach, California, 2016.
- [30] H. Deng, T. Li, Z. Wang, and X. Ma, "Pretension design of space mesh reflector antennas based on projection principle," *Journal of Aerospace Engineering*, vol. 28, article 04014142, 2014.
- [31] T. Li, Y. Tang, and T. Zhang, "Surface adjustment method for cable net structures considering measurement uncertainties," *Aerospace Science and Technology*, vol. 59, pp. 52–56, 2016.
- [32] S. Morterolle, B. Maurin, J. Quirant, and C. Dupuy, "Numerical form-finding of geotensoid tension truss for mesh reflector," *Acta Astronautica*, vol. 76, pp. 154–163, 2012.
- [33] W. Rusch and P. Potter, Analysis of reflector antennas, Academic Press, 111 Fifth Avenue, New York, NY 10003 & Berkeley Square House, London, WIX 6BA, 2013.
- [34] J. Nocedal and S. Wright, *Numerical Optimization*, Springer Science & Business Media, 233 Spring Street, New York, NY 10013, 2006.
- [35] S. Yuan and B. Yang, "Design and optimization of tension distribution for space deployable mesh reflectors," in *In: 26th AAS/AIAA Space Flight Mechanics Meeting*, pp. 765–776, Univelt Escondido, CA, 2016.
- [36] S. Yuan, B. Yang, and H. Fang, "Direct root-mean-square error for surface accuracy evaluation of large deployable mesh reflectors," in *In: AIAA SciTech 2020 Forum*, p. 935, Orlando, Florida, 2020.
- [37] S. Yuan, B. Yang, and H. Fang, "Self-standing truss with hard-point-enhanced large deployable mesh reflectors," *AIAA Journal*, vol. 57, no. 11, pp. 5014–5026, 2019.
- [38] S. Yuan, B. Yang, and H. Fang, "The projecting surface method for improvement of surface accuracy of large deployable mesh reflectors," *Acta Astronautica*, vol. 151, pp. 678–690, 2018.